A Metasurface-Based Low-Profile Array Decoupling Technology to Enhance Isolation in MIMO Antenna Systems

ZIYANG WANG[1,2], **(Member, IEEE), CHENGLEI LI**[1], **(Graduate Student Member, IEEE),**
QIONG WU[1,3], **(Member, IEEE), AND YINGZENG YIN**[2], **(Member, IEEE)**

[1]Beijing National Research Center for Information Science and Technology, Electronic Engineering Department, Tsinghua University, Beijing 100084, China
[2]National Key Laboratory of Antennas and Microwave Technology, Xidian University, Xi'an 710071, China
[3]Key Laboratory of Advanced Process Control for Light Industry, School of Internet of Things Engineering, Jiangnan University, Wuxi 214122, China

Corresponding author: Ziyang Wang (wangziyang1@tsinghua.edu.cn)

ABSTRACT In this paper, a metasurface-based coupling reduction method is presented with the advantage of low profile for the MIMO antenna array. Unlike other metasurface-based decoupling technologies, this proposed metasurface for decoupling is loaded in the same layer as the coupled two-element patch antennas. Hence, the profile of the proposed decoupled array is greatly reduced compared to that of other published metasurface-based decoupled arrays. In this design, the two patch antennas with a short edge-to-edge distance of approximately 0.06 λ are surrounded by the period split ring resonator (SRR) elements. Next, two prototypes are fabricated; the test results show that the isolation performance for the decoupled array is better than that of a coupled array without SRRs, and the value of |S21| improves from -8 dB to -25 dB in a wide band of 5.0-6.0 GHz with |S21| < -25 dB. The impedance matching bandwidths for two arrays without and with SRRs are approximately 700 MHz (12.7%) and 1500 MHz (27%), respectively, with |S11| < -10 dB. In other words, a high-isolation MIMO array with the advantages of a low profile and a compact size is realized. It is exciting that the peak gains for the proposed decoupled array are improved by approximately 2 dB in the entire working band range. In addition, the efficiencies of the decoupled array increase by 15% compared to those of the coupled array, and the envelope correlation coefficient (ECC) also greatly improves. Therefore, the signs suggest that this proposed metasurface-based decoupling method is an efficient measure for MIMO array applications in the future.

INDEX TERMS MIMO, low-profile, metasurface-based, split ring resonators (SRRs), decoupling.

I. INTRODUCTION

The demands for the high rate and average throughput have explosive growth, such as smart home life and internet of vehicles communication. Therefore, it has greatly promoted the development of wireless communication technology, especially the coming of the fifth generation (5G) mobile communication. Multiple-input multiple-output (MIMO) [1], [2] is the most promising technology that has been studied for several decades. Hence, the MIMO antenna array is widely utilized in many devices and applications [1]. Since miniaturization design of antennas is

The associate editor coordinating the review of this manuscript and approving it for publication was Davide Ramaccia.

required, the space at the base station end or in a mobile terminal is only a fraction of wavelengths in vacuum. Consequently, the mutual coupling between MIMO array elements fiercely increases, while the radiation capability [3] and data throughput [4] of the array are seriously affected. As a result, it is necessary to reduce the mutual coupling between antennas as much as possible [5], especially in compact arrays.

Many decoupling techniques [6]–[32] have attracted attention in academia and industry, not only the method to increase the physical separation of elements. Some conventional methods such as loading a T-type branch [6] or etching a decoupling slots on the ground floor [7] are proposed with a high isolation performance. Next, the neutralization line decoupling technology as an effective method for the

reduction of coupling is also investigated in depth. Even the proposed neutralization line decoupling technology can be used for three-frequencies decoupled antennas [8] and UWB high isolation MIMO antennas [9]. In addition, near-field resonators (NFR) as a novel decoupling technique for closely packed patch elements in MIMO antennas is proposed [10]. The decoupling network (DN) [11], [12] as an efficient approach for decoupling arrays. An eigen-mode method based on the inherent decoupling effect is utilized by feeding the orthogonal modes of the array to achieve port decoupling in [13]–[15]. A coupling resonator decoupling network (CRDN) as another network decoupling method is investigated systematically in [16]–[18]. It can work in mobile terminals [16] at single frequency, dual band decoupling antennas [17], and integrated with low-temperature co-fired ceramic (LTCC) technology in a wide operating band [18].

In recent years, the artificial electromagnetic material as an effective technology to control electromagnetic wave propagate is utilized in the decoupling design of MIMO array antennas. According to different positions of decoupling metamaterials, this decoupling method can be divided into three cases: metamaterial structures etched on the ground floor such as a defected ground structure (DGS), an electromagnetic band gap (EBG) between two coupling antennas, and a cover on the coupling arrays as SRRs. In the first case, in paper [19]–[21], a novel second or third iterative fractal DGS acting as an artificial structure is etched on the ground to suppress the mutual coupling between micro-strip antenna elements in [19]. Then, meander line slots using photolithography and electrodeposition technology [20] are etched on the ground plane to decrease the coupling. However, this etching method will cause undesirable backward radiation. In the second case, some researchers consider putting several period structures [22]–[25] between two coupled MIMO antennas. In [22], a novel H-shaped conducting wall is introduced between two closely spaced patch antennas with an edge-to-edge distance of 0.052 λ, and a high isolation parameter of approximately 50 dB is achieved. In paper [23], a six-parallel-metal-strips structure is printed on the substrate layer, which can be equivalent to a band stop filter to suppress the transmission of electromagnetic wave. In paper [25], another asymmetrical coplanar strip (ACPS) wall is used to suppress the coupling by introducing a coupling path. In addition, EBG [26], [27] as a special structure in the metamaterial field is also loaded between two adjacent antenna elements for the mutual coupling reduction. In paper [26], a fractal UC-EBG structure is introduced for decoupling. Nowadays, in the third case, there are more and more reports about the metasurface cover decoupling technology in academic [28]–[32]. In paper [28], a suspended metasurface consists of periodic square split ring resonators (SRRs) is proposed to decouple a MIMO array, where the isolation bandwidth can be effectively controlled by changing the range of negative permeability band. Afterwards, the proposed metasurface antenna array decoupling (MAAD) method is reported frequently.

Then, a metasurface cover consists of period short wires [29] is introduced for the array decoupling based on this proposed MAAD method. This metasurface-based method can be used in dual-band decoupling [30], [32] of MIMO arrays. In addition, two linearly polarized antennas can be decoupled in both H-plane and E-plane based on this proposed MAAD method [31] by properly designing the metasurface consisting of short wires. This novel decoupling technology is very productive, but these decoupled arrays have the disadvantage of high profile. Therefore, a much more effective approach should be investigated to decrease the profile of MIMO decoupled arrays in the future.

In this paper, a novel low-profile metasurface decoupling method is proposed. The coupled two-element antenna array is surrounded by period square split ring resonator elements, which is different from other metasurface-based decoupling methods that place a netasyrface between two coupled antennas or loading a metasurface cover above them. First, the electromagnetic characteristics of the SRR elements, design process and principle of this metasurface-based decoupling method are presented. Then, the electric fields, magnetic fields and Poynting vector distributions for the coupled and decoupled arrays in different planes are investigated in detail to clarify the decoupling performance by using the SRRs in the same layer. Key factors are analyzed to investigate the working mechanism. Thereafter, two prototype of arrays are fabricated, and the measured results show that the proposed decoupled array has better isolation performance than the coupled array, which can satisfy the requirements of both IEEE 802.11a (5.15-5.35GHz and 5.47-5.725GHz) American standard and HIPPER LAN/2 (5.15-5.35GHz and 5.725-5.825GHz) European standard. Other aspects for the decoupled array are also greatly improved. Therefore, it is a good candidate for decoupling of multiple-element arrays for wireless communication systems in future.

II. ANTENNA DESIGN FOR DECOUPLING AND ANALYSIS

In this section, the design and analysis of the proposed metasurface-based decoupling method with the advantage of low profile are presented in detail. First, the electromagnetic characteristics for the SRR elements are presented to clarify the decoupling mechanism in Fig. 1. The design process and the geometry structures for the proposed decoupled MIMO array antenna are presented as shown in Fig. 2. Then, brief analytics for the principle of coupling and decoupling are shown in Figs. 3 and 4. After that, the current and electric distributions on the surface for the coupled and decoupled arrays are shown in Figs. 5 and 6 to show the effect of decoupling by using these surrounding SRR elements. Meanwhile, the electric field, magnetic field and Poynting vector distributions on the section in the XOZ plane for two arrays are presented in Figs. 7, 8 and 9. Next, the key factors for decoupling are discussed in detail in Figs. 10, 11 and 12. Finally, the effectiveness of the proposed decoupling method is compared with the traditional measure by increasing the distance between two coupled antennas as shown in Fig. 13.
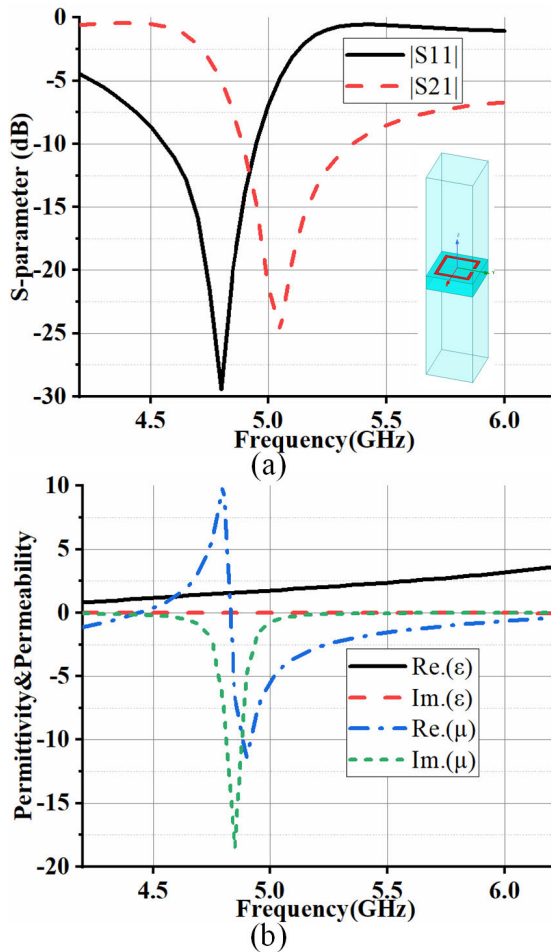
FIGURE 1. Characteristic of the proposed SRRs element, (a) S parameter of the unit, (b) the values of permittivity and permeability for the proposed element.

A. ANALYSIS OF THE ELEMENT AND DESIGN PROCESS

To briefly investigate the internal connection of this proposed SRRs for decoupling, the characteristic for SRRs is studied in Fig. 1. The S-parameters for the proposed period SRR elements are presented as shown in Fig. 1 (a). The permittivity and permeability are calculated based on the values of S-parameters, and their curves are shown in Fig. 1 (b). Moreover, it is clear that the real part of permeability is negative in the desired band, and the permittivity is positive. As we know, the propagation of energy will be attenuated in a single negative medium, while this phenomenon does not exist in ordinary media and double negative media. Thus, the undesired electromagnetic energy that propagates from antenna 1 to antenna 2 to cause the mutual coupling is weakened with the increase in transmission distance. Therefore, the mutual coupling between two element antennas array has been decreased by loading the SRR elements.

To reveal the evolution process of this low-profile decoupled method by using the metasurface, all antennas in the design process are presented as shown in Figs. 2 (a), (b) and (c). First, Array 1 is the two-element
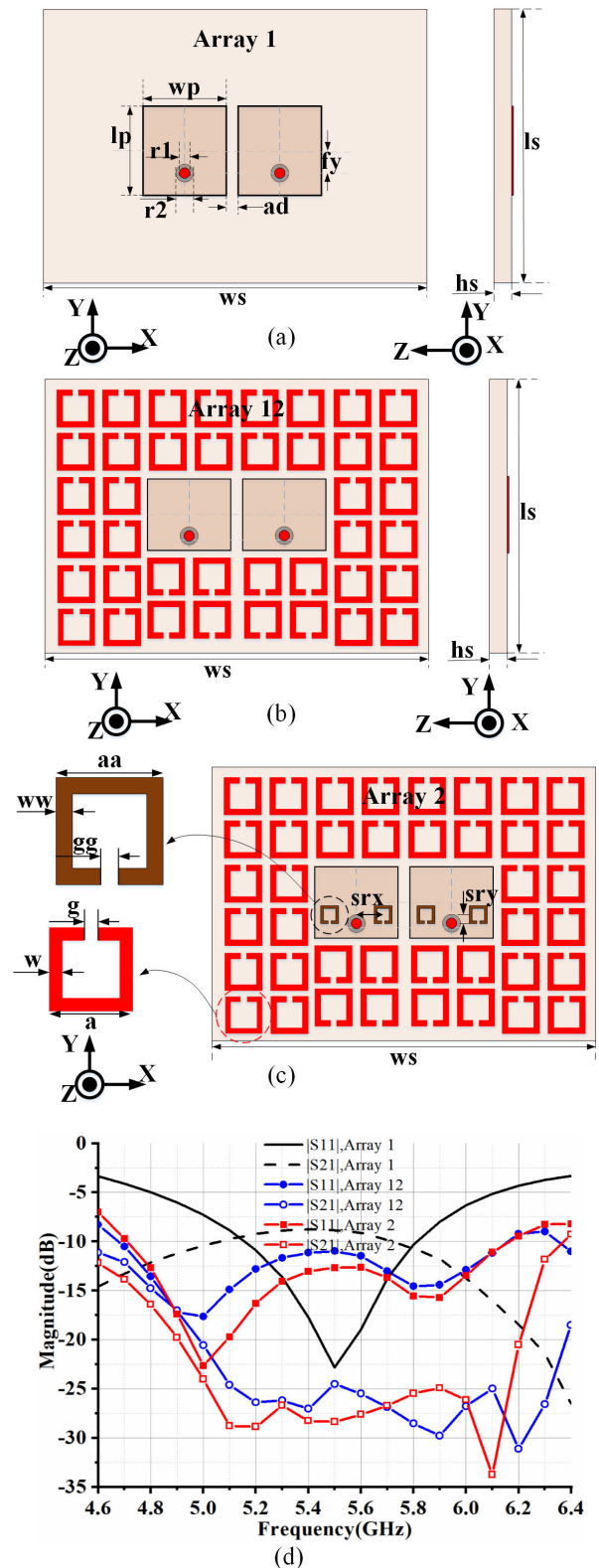

FIGURE 2. Geometry structure and corresponding S-parameters, (a) geometry structure of Array 1, (b) geometry structure of Array 2, (c) geometry structure of Array 3, (d) S parameter for the proposed Arrays.

coupled array with a common ground, and the geometry structure for the two coupled antennas with a close distance is shown in Fig. 2 (a). Moreover, the values of the S-parameter

for Array 1 are also presented in Fig. 2 (d), but the isolation performance of Array 1 is intolerable. Thereafter, the isolation structures are loaded around the coupled MIMO array in the same layer as shown in Fig. 2 (b) named Array 12, and |S21| has been greatly improved as shown in Fig. 2 (d). Then, in order to enhance the matching performance of Array 12, two pairs of small SRRs are etched on two rectangle patches, named Array 2. The value of |S11| for Array 2 has clearly improved without deteriorating the isolation performance especially in the high-frequency band, as shown in Fig. 2 (d). The geometry structure for Array 2 is presented in Fig. 2 (c).

Array 1 and Array 2 are both printed on the FR4 structure with a dielectric contains of 4.4, a loss tangent of 0.02, and a thickness of 3.0 mm. Thereafter, the structure of the proposed decoupled antenna is optimized and design by using the full wave simulation software HFSS 18. Then, the dimensions for the proposed decoupled array are as follows: ws=63 mm, ls=49 mm, hs=3 mm, wp=11.4 mm, lp=11 mm, r1=1.3 mm, r2=3 mm, fy=4 mm, ad=3.6 mm, a=6.4 mm, w=0.5 mm, g=1.2 mm, aa=3.3 mm, ww=0.5 mm, gg=1.2 mm, srx=3.0 mm, sry=1.5 mm.

Moreover, a wideband isolation performance for the decoupled array is achieved due to the loading SRRs in the same layer. There are two possible reasons for this decoupling performance. First, an isolation bandwidth for the range of negative permeability is generated by the period SRRs, which can depress the mutual coupling as described in Fig. 1 (b). Next, the loading four SRRs with different rotation directions as shown in Fig. 10 break the periodicity electromagnetic characteristics of SRRs, which is different from the previous strictly periodic SRR elements, and it can participate in parasitic radiating for decoupling. Hence, the isolation bandwidth of Array 2 is clearly wider than Array 3 from the simulated results in Fig. 11.

As we know, two pairs of SRR slots etched on two patches can broaden the bandwidth of |S11|. More important, the matching performance can be improved by properly rotating some opening directions of SRRs around two patches. The comparison of the values of |S11| for Array 2 with Array 4 is shown in Fig. 11. In fact, the dual-mode of TM10 and TM21 resonance is achieved. Therefore, it is reasonable that the matching bandwidth is broadened with the common effects of loading the parasitic SRR elements and etching the small SRRs slots on the two aforementioned patches.

B. DECOUPLING PRINCIPLE FOR THE PROPOSED METHOD

According to the above conclusion, the schematic diagrams of the mutual coupling for coupled and decoupled arrays are shown in Figs. 3 and 4, respectively. In Fig. 3, when antenna 1 is excited, the energy will be coupled to antenna 2. Moreover, according to different paths of propagation, the energy coupled to antenna 2 can be divided into two parts, one is the energy coupled to antenna 2 through space called space wave coupling, the other is the energy coupled to antenna 2
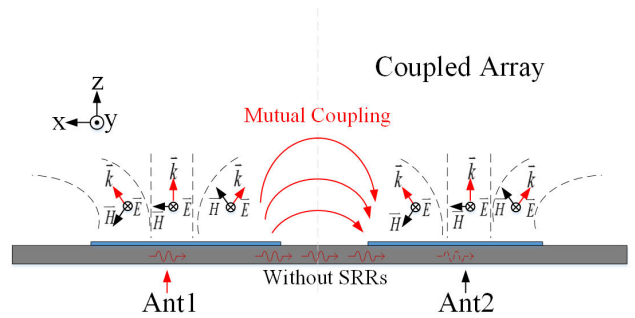

FIGURE 3. Diagrammatic sketch of the coupled array without SRRs.
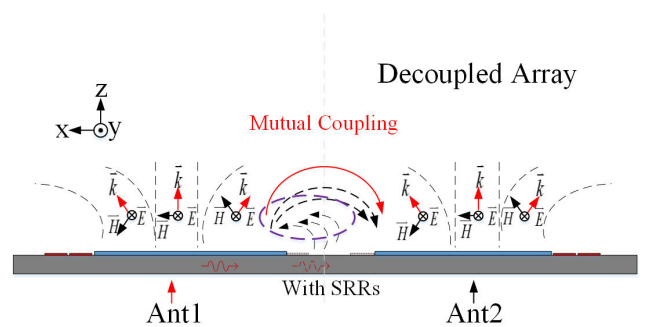

FIGURE 4. Principle of the proposed decoupled array with SRRs.

in medium called surface wave coupling. Because of the strong coupling between these two elements, the radiation performance of array sharply deteriorates. In addition, the space wave coupling is characterized by the red solid line when antenna 1 is excited, and the surface wave coupling is characterized by the red curve in the medium in Fig. 3 from antenna 1 to antenna 2. Then, the sever SRRs are loaded around two nearby patches as shown in Fig. 4, the coupling is greatly suppressed. On the one hand, the parasitic SRR elements loaded in the same layer also participate in the radiation. Meanwhile, the radiation direction of some parasitic elements is reversed with the coupling energy from antenna 1 to antenna 2, which can offset part of the coupling energy as shown in the purple circle area in Fig. 4. Therefore, the space wave coupling greatly decreases. On the other hand, the surface wave coupling has also been reduced due to the presence of the SRR decoupling structures, although it does not occupy the main coupling effect. In short, the mutual coupling between two closely antennas have been reduced using the proposed metasurface-based decoupling method.

C. CURRENT AND FIELD ANALYSIS ON SURFACE

Moreover, to reveal the working principle of the proposed decoupled MIMO antenna, the current distributions on the patches with and without the surrounding SRRs are shown in Fig. 5. When antenna 1 is excited in Fig. 5 (a), an induced current is introduced to antenna 2. Therefore, the mutual coupling between two antennas is very strong, which will seriously affect the independent radiation of antenna 2 in
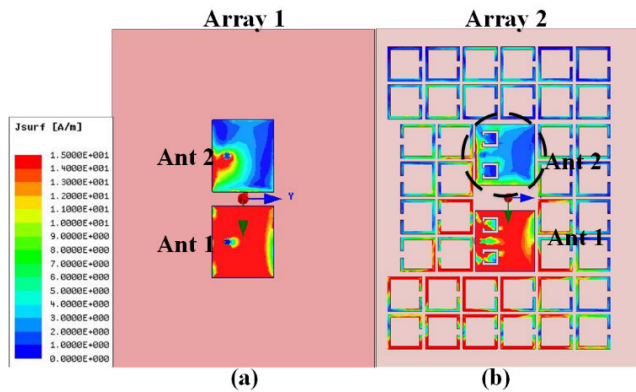
FIGURE 5. Surface current distributions on the surface of two arrays with and without SRRs in the XOY plane.

the coupled array. Then, several SRRs are loaded around the coupled array, and the coupling current is introduced to the adjacent SRR elements, which is opposite to the direction of mutual coupling current, as shown in Fig. 5 (b). In other words, the direction of antenna 1 radiating to the parasitic SRRs is the opposite of the direction of antenna 1 coupling to antenna 2, so the energy radiating from parasitic SRRs offsets to the energy coupling from antenna 1 to antenna 2. Therefore, the isolation performance between the two-element array greatly improves.

In addition, in order to further investigate the isolation effect of the proposed decoupling method using SRRs, the electric field distributions on the surface are also presented for different arrays in the XOY plane. As shown in Fig. 6 (a), when antenna 1 is excited, the electric field coupling to the patch of antenna 2 is strong. Thereafter, with SRRs loading around the two coupled patches at the same layer, the electric field is dispersed over the surrounding metal SRRs.
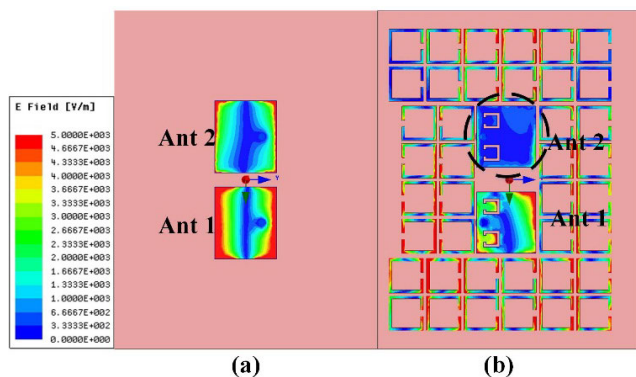

FIGURE 6. Simulated electric field distributions on the surface of two arrays with and without SRRs in the XOY plane.

Obviously, there is no electric field distribution on the patch of antenna 2 as shown in Fig. 6 (b). In other words, only a small amount of energy is coupled to antenna 2 with the loading of SRRs when antenna 1 is excited. Therefore, the proposed decoupling method is very effective.

D. FIELD DISTRIBUTIONS ON THE XOZ PLANE

The current and electric field distributions on the surface have been presented in the previous chapter. To more clearly explore the decoupling performance, the section distributions of electric field, magnetic field and Poynting vector on the XOZ plane are also shown, and the simulated results are obtained by the full wave software HFSS 18.

The contours of the electric field for the arrays without and with SRRs on XOZ plane are shown in Figs. 7 (a) and (b). In the two cases of arrays, antenna 1 is excited, while antenna 2 is terminated with 50-Ohm matched loading. The electric field from antenna 1 radiates to antenna 2 at region A in the coupled array, as shown in Fig. 7 (a). With the loading of SRRs, the coupling electric field above antenna 2 fiercely decreases in region B, as shown in Fig. 7 (b). This result is also consistent with Fig. 9 (b). The corresponding vector magnetic field distributions on the same section for different arrays without and with SRRs are also presented as shown in Fig. 8.
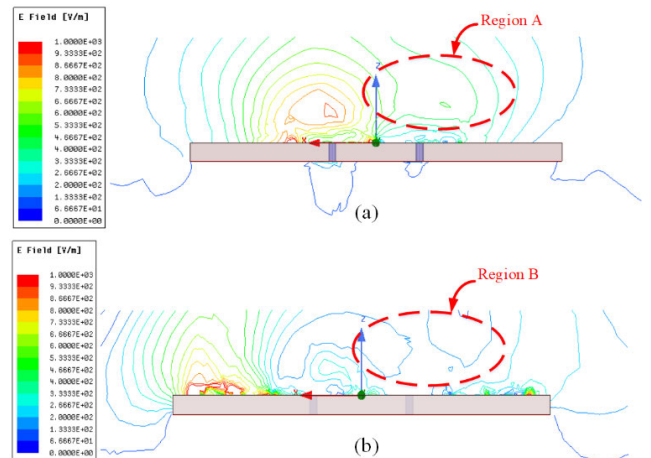

FIGURE 7. (a) Simulated electric field contours on a cutting surface in the XOZ plane for the coupled array without SRRs, (b) Simulated electric field contours on a cutting surface in the XOZ plane for the decoupled array with SRRs.

In the end, the simulated Poynting vector distributions on a cutting surface for the two arrays in the XOZ plane are presented to clarify the energy flow. As shown in Fig. 9 (a), the energy from antenna 1 spreads in the 3D space, and the mutual coupling emerges since the energy flows to antenna 2 in Region A' of the coupled array. Thereafter, the SRRs are loaded surrounding the two antennas, and the coupling energy is greatly reduced as shown in Fig. 9 (b) in Region B'. Less energy is radiated into antenna 2 with antenna 1 at the excited state for the decoupled array. Therefore, the mutual coupling is significantly reduced with the loading of SRRs in the same layer as shown in Figs. 7, 8 and 9.

E. PARAMETRIC STUDIES

Some key parametric studies are conducted to analyze the electromagnetic response with different situations. First, the opening rotate directions of SRRs on both sides are
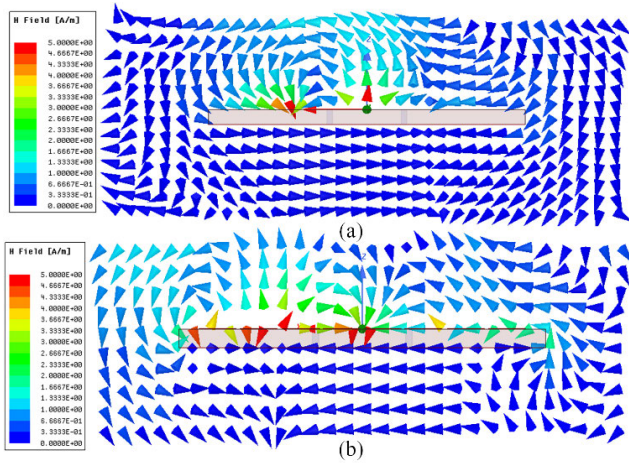
FIGURE 8. (a) Simulated vector magnetic field distribution on a cutting surface in the XOZ plane for the coupled array without SRRs, (b) Simulated vector magnetic field distribution on a cutting surface in the XOZ plane for the decoupled array with SRRs.
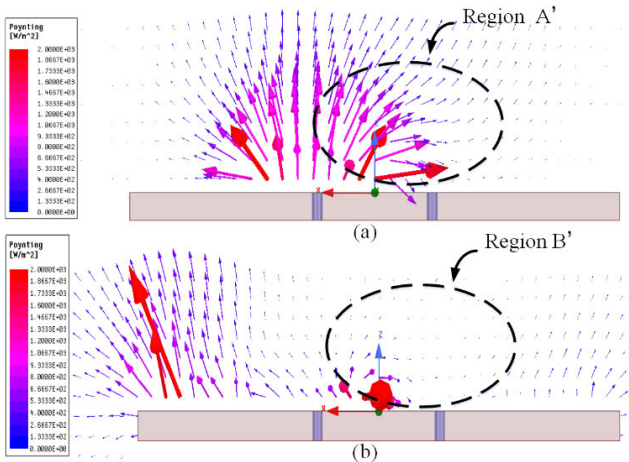

FIGURE 9. (a) Simulated Poynting vector distribution on a cutting surface in the XOZ plane for the coupled array without SRRs, (b) Simulated Poynting vector distribution on a cutting surface in the XOZ plane for the decoupled array with SRRs.

discussed for the three cases. As shown in Fig. 10 (a), Array 2 is the proposed decoupled array, and the opening directions of SRRs on both sides of two patches are opposite. Next, the opening directions of SRRs on Array 3 are identical, as shown in Fig. 10 (b). For Array 4, the opening directions of SRRs on both sides are perpendicular to each other as shown in Fig. 10 (c).

Then, the simulated S-parameters corresponding to these three cases are also presented in Fig. 11. It should be noted that Array 2 is the proposed array, and Array 3 is surrounded by the strictly periodic SRRs with identical opening directions, which are regularly utilized. As shown in Fig. 11, the isolation bandwidth of |S21| for Array 3 is smaller than the proposed Array 2 in this paper; meanwhile, the |S11| curve of Array 2 is identical to that of Array 3. Since the loading SRRs with different opening directions has the function
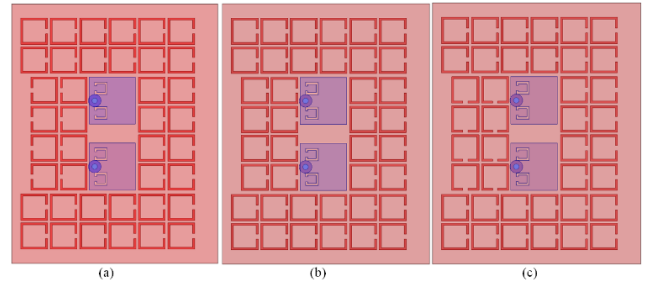

FIGURE 10. (a) Array 2, the proposed array, opposite opening directions of SRRs on both sides (b) Array 3, the identical opening directions of SRRs on both sides, (c) Array 4, perpendicular opening directions of SRRs on both sides.
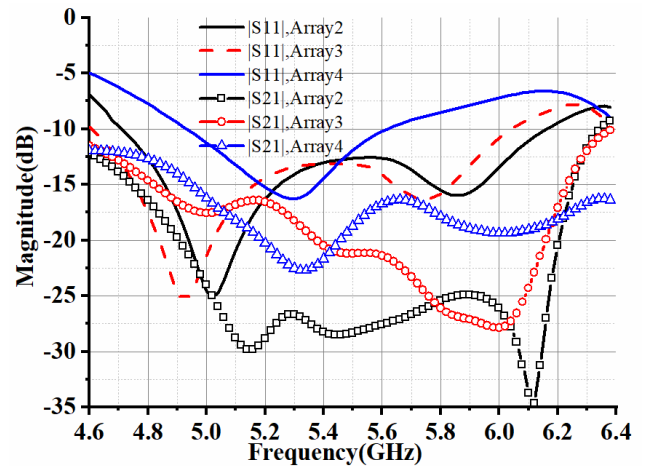

FIGURE 11. Simulated S-parameters for Array 2, Array 3 and Array 4, corresponding to Fig. 10.

of parasitic radiating, it is essential to a reasonable design for a good isolation performance. In addition, the matching performance of the decoupled array will also be harshly affected by the rotate directions of opening for SRRs, comparing the values of Array 2 with Array 4. Therefore, it is necessary to investigate the opening directions of SRRs.

Then, the effect for the length of SRRs is investigated as shown in Fig. 12. The size of SRRs is sensitive because of the response frequency band elaborated in Figs. 1 (a) and (b). Moreover, the isolation bandwidth moves to low frequencies when parameter "a" increases, while it will move to high frequency band when parameter a decreases. It is also consistent with our common sense.

F. COMPARISON OF ISOLATION PERFORMANCE
In order to quantify the effectiveness of the proposed low profile decoupling method by using the surrounding SRRs in the same layer, the values of |S21| for the coupled arrays with different edge-to-edge spaces are investigated in Fig. 13. Moreover, the isolation curve for the proposed decoupled array loading SRRs is added with a short element distance of approximately 0.06 λ. This metasurface-based decoupling method is very powerful compared with to the traditional
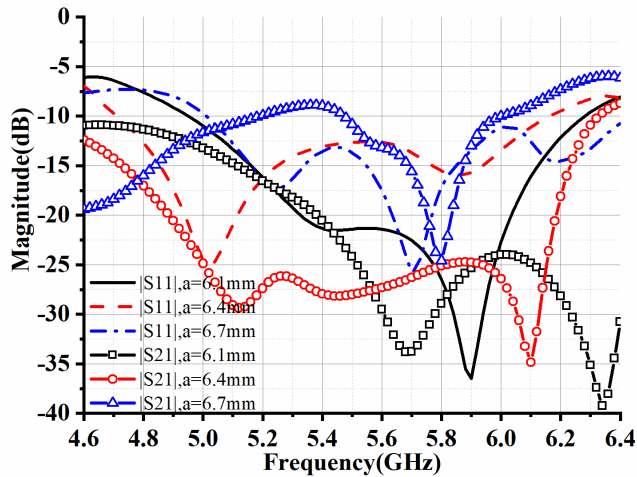
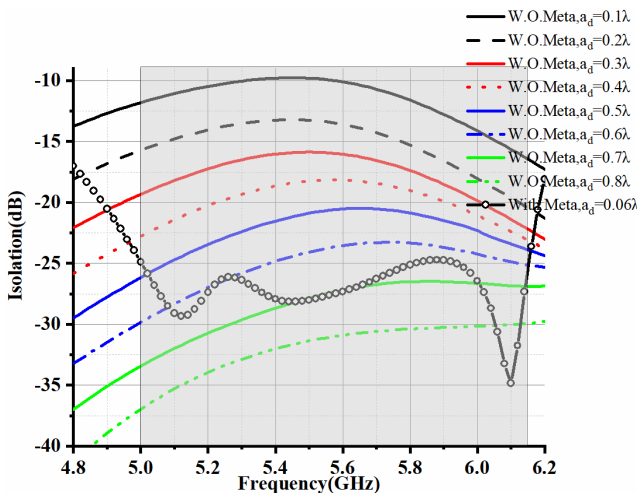**FIGURE 12.** Simulated S-parameters of Array 2 for different a values, which are the length of the SRRs.

FIGURE 14. Simulated and measured S parameters for the coupled array without SRRs.

FIGURE 13. Simulated isolation curves for arrays with different ad values compared to the proposed decoupled array.
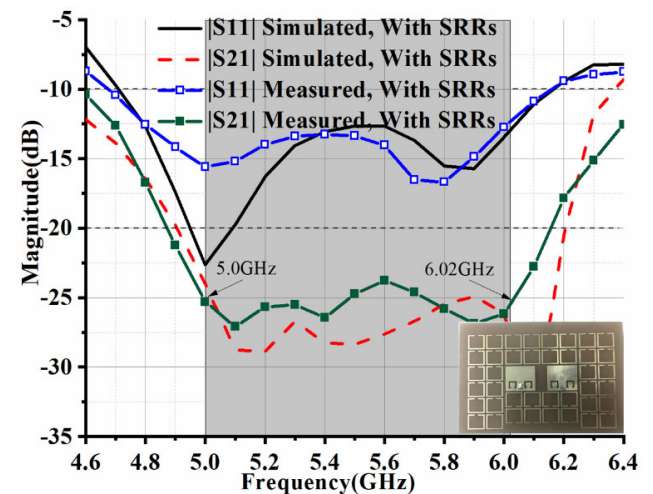
FIGURE 15. Simulated and measured S parameters for the decoupled array with SRRs.

method. The equivalent isolation effect can be obtained by the coupled antennas without SRRs, unless the distance between the two coupled antennas is at least 10-12 times (0.6 λ - 0.7 λ) larger than before.

III. EXPERIMENTAL RESULTS AND DISCUSSION
A. SCATTERING PERFORMANCE

The prototypes for the proposed MIMO arrays with and without SRRs are shown in Figs. 14 and 15. The simulated and measured S parameters for the two proposed MIMO array antennas are also presented in Figs. 14 and 15, respectively. Good consistent is obtained between simulated and measured results for the coupled and decoupled arrays. The matching bandwidth for the coupled MIMO array is approximately 700 MHz for |S11| below −10 dB. Meanwhile, the isolation performance for the coupled MIMO array without SRRs is intolerable. However, |S21| improves from −8 dB to −25 dB in a wideband of 5.0-6.0 GHz by using the proposed metasurface-based decoupling technology. In addition, the
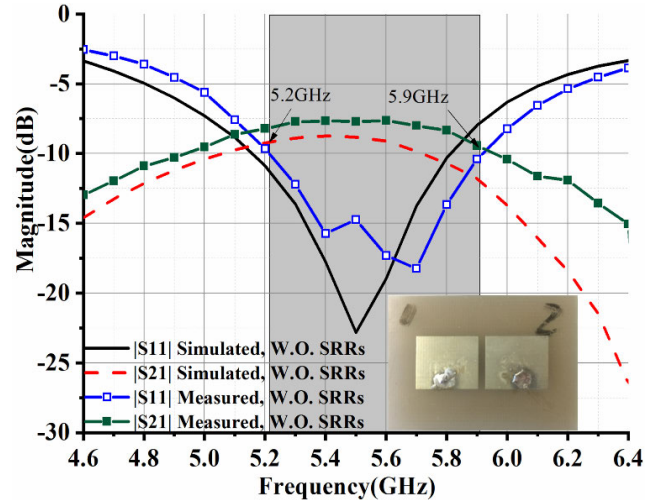
matching bandwidth for the proposed decoupled array has also been increased to the 1500-MHz range from 4.7 GHz to 6.2 GHz with the |S11| below −10 dB, and it is wider than before. Therefore, a good measured performance for the decoupled array is realized in the desire band of 5.0-6.0 GHz using the proposed decoupling structures.

B. RADIATION PERFORMANCE

To further investigate the radiation performance for the coupled and decoupled MIMO antenna arrays, the simulated and measured far-field radiation patterns of the co- and cross- polarization are presented with different ports excited at different frequency points in different planes, as shown in Figs. 16 and 17. The results for the coupled array are shown in Fig. 16, while the data for the decoupled array are shown in Fig. 17. The patterns for two arrays with port 1 in the excited state are shown in Figs. 16 (a, c) and 17 (a, c), while others are excited by port 2. In addition, the patterns at
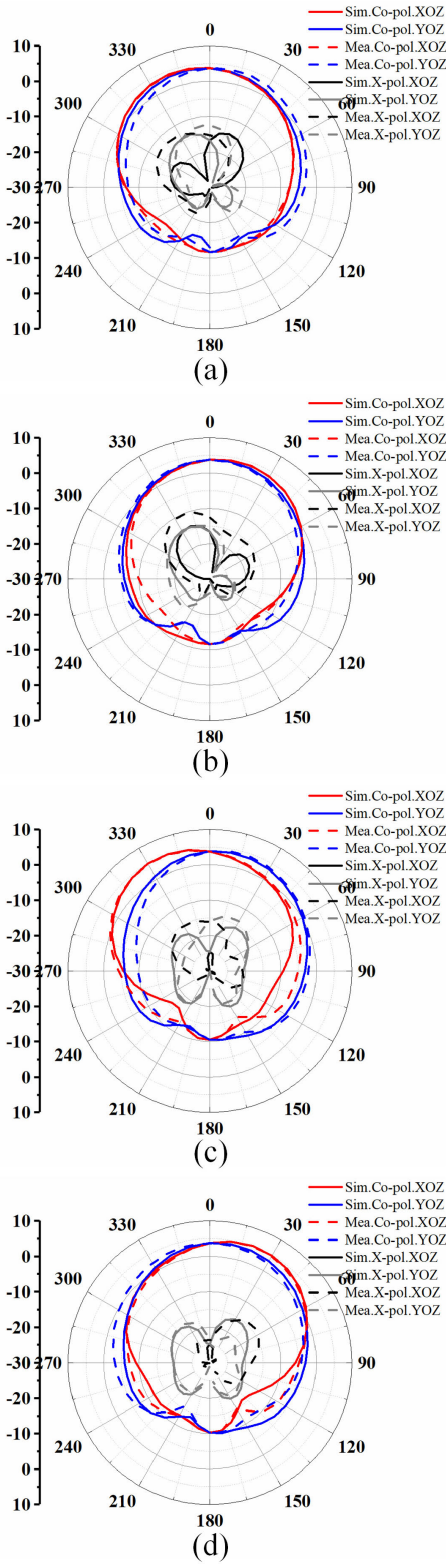
FIGURE 16. Simulated and measured radiation patterns of co- and cross polarization in different plans for the coupled array, (a) 5.2 GHz with port 1 excited, (b) 5.2 GHz with port 2 excited, (c) 5.8 GHz with port 1 excited, (d) 5.8 GHz with port 2 excited.

FIGURE 17. Simulated and measured radiation patterns of co- and cross polarization in different plans for the decoupled array, (a) 5.2 GHz with port 1 excited, (b) 5.2 GHz with port 2 excited, (c) 5.8 GHz with port 1 excited, (d) 5.8 GHz with port 2 excited.

5.2 GHz are presented in Figs. 16 (a, b) and 17 (a, b), and the others are the case of 5.8 GHz. It is obvious that the pattern performance is stable in the entire working band.
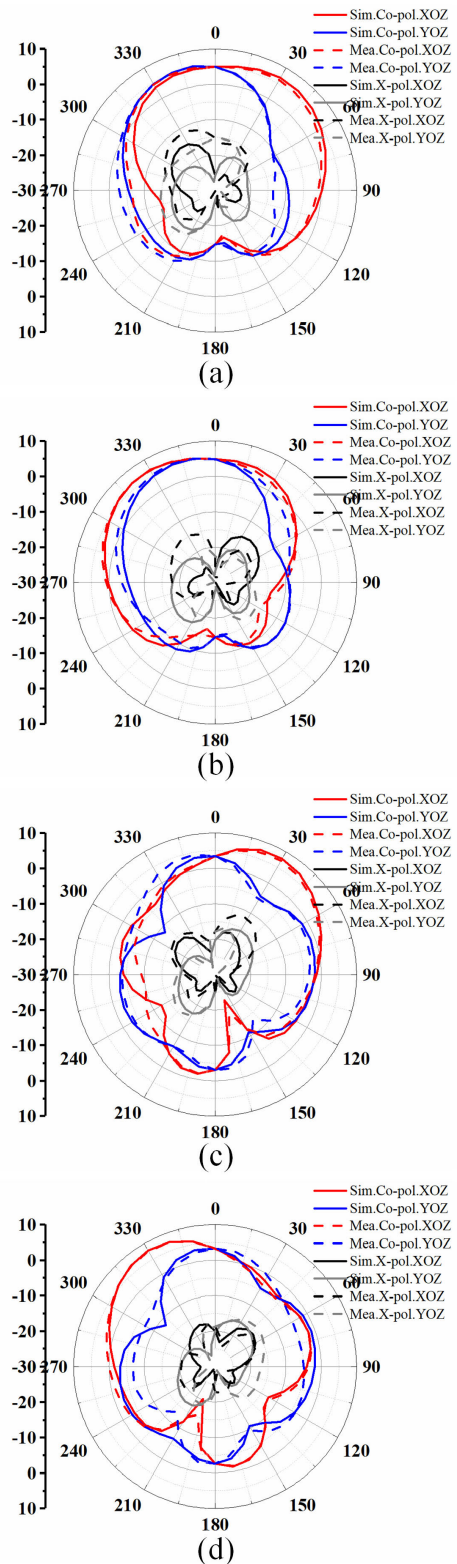
Moreover, the peck gains for the two different arrays are also surveyed. Since the array radiation aperture is greatly increased with the loading of SRRs in the same layer, the peck
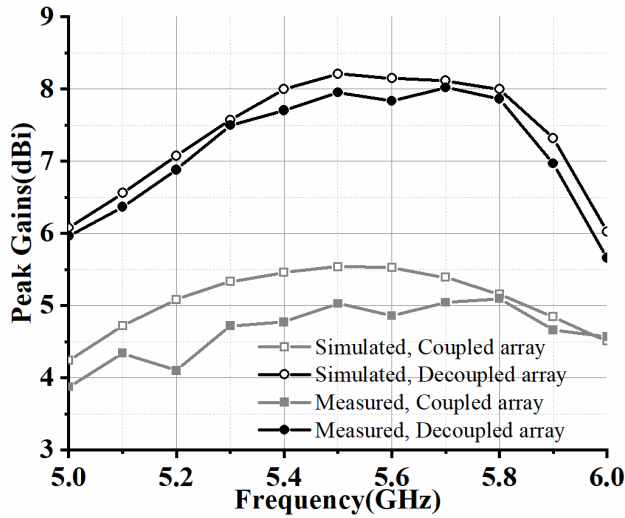
FIGURE 18. Simulated and measured peak gains of the two proposed arrays with and without SRRs.
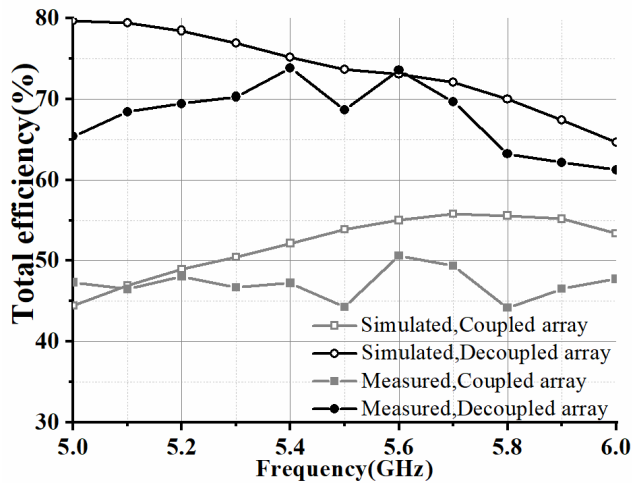

FIGURE 19. Simulated and measured efficiencies of the two proposed arrays with and without SRRs.

FIGURE 20. ECC for the proposed coupled and decoupled arrays.

$$\vec{E_1}(\theta, \phi) \cdot \vec{E_2}(\theta, \phi)$$
$$= \vec{E}_{\theta 1}(\theta, \phi) \vec{E}^{*}_{\theta 2}(\theta, \phi) + \vec{E}_{\phi 1}(\theta, \phi) \vec{E}^{*}_{\phi 2}(\theta, \phi) \quad (2)$$

$\vec{E_i}(\theta, \phi)$ is the measured electric filed vector of antenna i with another antenna terminated by a 50-Ω load. The values of the ECC are calculated by Formula. 1 and improved from 0.2 to 0.05. Therefore, it is an effective method to improve the isolation performance for the coupled array. A larger channel capacity and diversity gain will be realized in the desire band.

D. COMPARISON WITH THE REFERENCED ANTENNA

The design of high isolation for MIMO arrays with the performance of the wideband is a technical difficulty in recent years. In [10], the novel near-field resonator (NFR) decoupling technology is presented with an excellent isolation performance at small edge separation and height, but the beautiful isolation bandwidth is incomplete. The novel fence-type decoupling structure [33] and neutralization line [9] are used for the decoupling of the wideband. However, the metasurface-based method is rarely reported to realize a broadband decoupling design. Dual-band decoupling for MIMO antennas by using a metasurface structure was reported in [30], [32]. Then, the resonant frequency, |S21| value, edge-to-edge distance for two antennas, and height of the array are compared with the referenced antennas in Table 1. Compared with the referenced antennas [28], [30], and [32], which used the same metasurface decoupling method, the proposed decoupled array has a wide bandwidth of isolation. Moreover, the proposed decoupled array has a lower height than other decoupled antennas based on the metasurface technology, since there is no surface above the coupled antennas. In addition, the edge-to-edge distance is smaller than other approaches as loading a Fence-Type decoupling structure between two antennas, and the center-to-center spacing is approximately 0.28 λ0, which is also small among similar decoupled arrays. Therefore, this

gains of the proposed decoupled array will be improved. As shown in Fig. 18, the peak gains for the decoupled array with SRRs have been improved more than that for the coupled array by approximately 2.0 dB in the entire band.

In addition, the efficiencies for the decoupled array with SRRs are approximately 15% higher than that of the coupled array as shown in Fig. 19. Therefore, based on the results of patterns, gains and efficiencies, the far-field radiation performance has been greatly improved in the entire desire broadband range of 5.0-6.0 GHz.

C. ENVELOPE CORRELATION COEFFIEICENT

As shown in Fig. 20, the ECC is investigated as an important parameter of the MIMO array system.

$$\rho_e = \frac{\left| \iint\limits_{4\pi} [\vec{E_1}(\theta, \phi) \cdot \vec{E_2}(\theta, \phi)] d\Omega \right|^2}{\iint\limits_{4\pi} |\vec{E_1}(\theta, \phi)|^2 d\Omega \iint\limits_{4\pi} |\vec{E_2}(\theta, \phi)|^2 d\Omega} \quad (1)$$
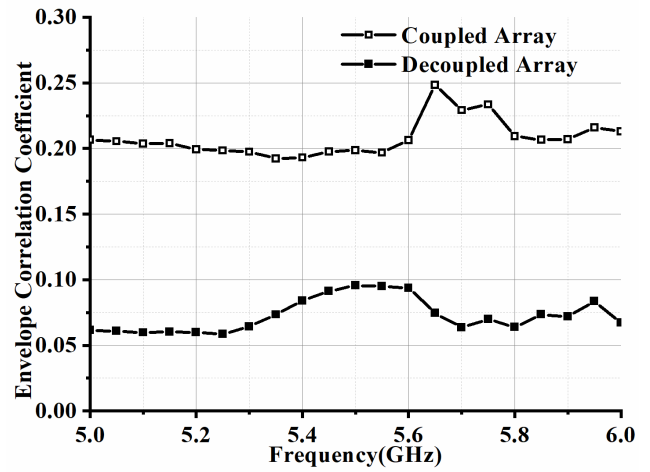
TABLE 1. Comparisons of the proposed antenna with the referenced antennas.

Ant	Method	Freq (GHz)	|S21| (dB)	E-E (λ_0)	Height (λ_0)
[10]	NFR	2.36-2.5	-20	0.016	0.024
[33]	Fence-Type	3.0-3.4	-25	0.35	0.01
[9]	Neutralization Line	3.1-5.0	-22	0.037	0.013
[28]	MAAD	5.6-6.1	-25	0.017	0.17
[30]	MAAD	2.6/3.5	-26/-14	0.01	0.13
[32]	MDM	3.7/4.1	-28/-25	0.034	0.3
Pro.	This method	5.0-6.0	-25	0.06	0.05

Notes: E-E represents the edge-to-edge distance for the decoupled array, and the value for the case of dual-bands is calculated according to the high-frequency point.

method of adopting a metasurface at the same layer with the two patches is effective for decoupling in MIMO antennas.

IV. CONCLUSION

In this paper, a novel low-profile decoupling method with metamaterial structures in the same layer as the coupled array is proposed. First, the characteristics of the SRR elements, design process and working mechanism for the proposed decoupled array are briefly presented. Then, electric fields, magnetic fields and Poynting vector distributions for the coupled and decoupled arrays are compared and analyzed in detail to show the decoupling effects of the metasurface. Key factors for the decoupling are analyzed, and the equivalent isolation effect can be realized on the coupled antennas with a distance of 12 times larger than previously achieved. Next, the experimental results show that the isolation performance is greatly improved from -8 dB to -25 dB in a wide band of 5.0-6.0 GHz. That is to say, the wideband high-isolation MIMO array with the advantages of a low-profile and a compact size is realized using the metasurface-based decoupling method. In addition, the peck gains have been improved by approximately 2.0 dB compared with those of the coupled array, and the efficiencies for the decoupled array are approximately about 15% higher than those achieved previously. The ECC as a key parameter for MIMO systems has also been improved from 0.2 to 0.05. Therefore, the proposed decoupling method has great potential for large-scale MIMO antenna systems in future.

REFERENCES

[1] M. A. Jensen and J. W. Wallace, "A review of antennas and propagation for MIMO wireless communications," *IEEE Trans. Antennas Propag.*, vol. 52, no. 11, pp. 2810–2824, Nov. 2004.

[2] E. G. Larsson, O. Edfors, F. Tufvesson, and T. L. Marzetta, "Massive MIMO for next generation wireless systems," *IEEE Commun. Mag.*, vol. 52, no. 2, pp. 186–195, Feb. 2014.

[3] H. Steyskal and J. S. Herd, "Mutual coupling compensation in small array antennas," *IEEE Trans. Antennas Propag.*, vol. 38, no. 12, pp. 1971–1975, Dec. 1990.

[4] L. Lu, G. Y. Li, A. L. Swindlehurst, A. Ashikhmin, and R. Zhang, "An overview of massive MIMO: Benefits and challenges," *IEEE J. Sel. Topics Signal Process.*, vol. 8, no. 5, pp. 742–758, Oct. 2014.

[5] H. Zou, Y. Li, B. Xu, Y. Chen, H. Jin, G. Yang, and Y. Luo, "Dual-functional MIMO antenna array with high isolation for 5G/WLAN applications in smartphones," *IEEE Access*, vol. 7, pp. 167470–167480, 2019.

[6] K.-L. Wong, C.-H. Chang, B. Chen, and S. Yang, "Three-antenna MIMO system for WLAN operation in a PDA phone," *Microw. Opt. Technol. Lett.*, vol. 48, no. 7, pp. 1238–1242, Jul. 2006.

[7] J. OuYang, F. Yang, and Z. M. Wang, "Reducing mutual coupling of closely spaced microstrip MIMO antennas for WLAN application," *IEEE Antennas Wireless Propag. Lett.*, vol. 10, pp. 310–313, 2011.

[8] Y. Wang and Z. Du, "A wideband printed dual-antenna with three neutralization lines for mobile terminals," *IEEE Trans. Antennas Propag.*, vol. 62, no. 3, pp. 1495–1500, Mar. 2014.

[9] S. Zhang and G. F. Pedersen, "Mutual coupling reduction for UWB MIMO antennas with a wideband neutralization line," *IEEE Antennas Wireless Propag. Lett.*, vol. 15, pp. 166–169, 2016.

[10] M. Li, B. G. Zhong, and S. W. Cheung, "Isolation enhancement for MIMO patch antennas using near-field resonators as coupling-mode transducers," *IEEE Trans. Antennas Propag.*, vol. 67, no. 2, pp. 755–764, Feb. 2019.

[11] M. Li, L. Jiang, and K. L. Yeung, "Novel and efficient parasitic decoupling network for closely coupled antennas," *IEEE Trans. Antennas Propag.*, vol. 67, no. 6, pp. 3574–3585, Jun. 2019.

[12] M. Li, L. Jiang, and K. L. Yeung, "A novel wideband decoupling network for two antennas based on the wilkinson power divider," *IEEE Trans. Antennas Propag.*, early access, Mar. 24, 2020, doi: 10.1109/TAP.2020.2981679.

[13] K. Wang, L. Li, and T. F. Eibert, "Comparison of compact monopole antenna arrays with eigenmode excitation and multiport conjugate matching," *IEEE Trans. Antennas Propag.*, vol. 61, no. 8, pp. 4054–4062, Aug. 2013.

[14] J. C. Coetzee and Y. Yu, "Port decoupling for small arrays by means of an eigenmode feed network," *IEEE Trans. Antennas Propag.*, vol. 56, no. 6, pp. 1587–1593, Jun. 2008.

[15] L. K. Yeung and Y. E. Wang, "Mode-based beamforming arrays for miniaturized platforms," *IEEE Trans. Microw. Theory Techn.*, vol. 57, no. 1, pp. 45–52, Jan. 2009.

[16] L. Zhao, L. K. Yeung, and K.-L. Wu, "A coupled resonator decoupling network for two-element compact antenna arrays in mobile terminals," *IEEE Trans. Antennas Propag.*, vol. 62, no. 5, pp. 2767–2776, May 2014.

[17] L. Zhao and K.-L. Wu, "A dual-band coupled resonator decoupling network for two coupled antennas," *IEEE Trans. Antennas Propag.*, vol. 63, no. 7, pp. 2843–2850, Jul. 2015.

[18] K. Qian, L. Zhao, and K.-L. Wu, "An LTCC coupled resonator decoupling network for two antennas," *IEEE Trans. Microw. Theory Techn.*, vol. 63, no. 10, pp. 3199–3207, Oct. 2015.

[19] K. Wei, J.-Y. Li, L. Wang, Z.-J. Xing, and R. Xu, "Mutual coupling reduction by novel fractal defected ground structure bandgap filter," *IEEE Trans. Antennas Propag.*, vol. 64, no. 10, pp. 4328–4335, Oct. 2016.

[20] S. Hwangbo, H. Y. Yang, and Y.-K. Yoon, "Mutual coupling reduction using micromachined complementary meander-line slots for a patch array antenna," *IEEE Antennas Wireless Propag. Lett.*, vol. 16, pp. 1667–1670, 2017.

[21] Z. Niu, H. Zhang, Q. Chen, and T. Zhong, "Isolation enhancement for 1×3 closely spaced E-plane patch antenna array using defect ground structure and metal-vias," *IEEE Access*, vol. 7, pp. 119375–119383, 2019.

[22] C.-H. Park and H.-W. Son, "Mutual coupling reduction between closely spaced microstrip antennas by means of H-shaped conducting wall," *Electron. Lett.*, vol. 52, no. 13, pp. 1093–1094, Jun. 2016.

[23] X.-B. Sun and M. Y. Cao, "Low mutual coupling antenna array for WLAN application," *Electron. Lett.*, vol. 53, no. 6, pp. 368–370, Mar. 2017.

[24] Y.-F. Cheng, X. Ding, W. Shao, and B.-Z. Wang, "Reduction of mutual coupling between patch antennas using a polarization-conversion isolator," *IEEE Antennas Wireless Propag. Lett.*, vol. 16, pp. 1257–1260, 2017.

[25] H. Qi, L. Liu, X. Yin, H. Zhao, and W. J. Kulesza, "Mutual coupling suppression between two closely spaced microstrip antennas with an asymmetrical coplanar strip wall," *IEEE Antennas Wireless Propag. Lett.*, vol. 15, pp. 191–194, 2016.

[26] X. Yang, Y. Liu, Y.-X. Xu, and S.-X. Gong, "Isolation enhancement in patch antenna array with fractal UC-EBG structure and cross slot," *IEEE Antennas Wireless Propag. Lett.*, vol. 16, pp. 2175–2178, 2017.

[27] M. Mavridou, A. P. Feresidis, and P. Gardner, "Tunable double-layer EBG structures and application to antenna isolation," *IEEE Trans. Antennas Propag.*, vol. 64, no. 1, pp. 70–79, Jan. 2016.

[28] Z. Wang, L. Zhao, Y. Cai, S. Zheng, and Y. Yin, "A meta-surface antenna array decoupling (MAAD) method for mutual coupling reduction in a MIMO antenna system," *Sci. Rep.*, vol. 8, no. 1, p. 3152, Dec. 2018.

[29] F. Liu, J. Guo, L. Zhao, X. Shen, and Y. Yin, "A meta-surface decoupling method for two linear polarized antenna array in sub-6 GHz base station applications," *IEEE Access*, vol. 7, pp. 2759–2768, 2018.

[30] F. Liu, J. Guo, L. Zhao, G.-L. Huang, Y. Li, and Y. Yin, "Dual-band metasurface-based decoupling method for two closely packed Dual-band antennas," *IEEE Trans. Antennas Propag.*, vol. 68, no. 1, pp. 552–557, Jan. 2020.

[31] J. Guo, F. Liu, L. Zhao, Y. Yin, G.-L. Huang, and Y. Li, "Meta-surface antenna array decoupling designs for two linear polarized antennas coupled in H-Plane and E-Plane," *IEEE Access*, vol. 7, pp. 100442–100452, 2019.

[32] Z. Niu, H. Zhang, Q. Chen, and T. Zhong, "Isolation enhancement in closely coupled dual-band MIMO patch antennas," *IEEE Antennas Wireless Propag. Lett.*, vol. 18, no. 8, pp. 1686–1690, Aug. 2019.

[33] L. Wang, Z. Du, H. Yang, R. Ma, Y. Zhao, X. Cui, and X. Xi, "Compact UWB MIMO antenna with high isolation using fence-type decoupling structure," *IEEE Antennas Wireless Propag. Lett.*, vol. 18, no. 8, pp. 1641–1645, Aug. 2019.

CHENGLEI LI (Graduate Student Member, IEEE) received the B.S. degree from the University of Electronic and Science Technology of China, Chengdu, China, in 2017. He is currently pursuing the M.S. degree with the Department of Electronic Engineering, Tsinghua University, Beijing, China. His current research interests include isoflux beamforming technology, genetic algorithm in electromagnetics, and reconfigurable reflectarray antenna.

QIONG WU (Member, IEEE) received the Ph.D. degree in information and communication engineering from the National Mobile Communications Research Laboratory, Southeast University, Nanjing, China, in 2016. He is currently a Lecturer with the School of Internet of Things Engineering, Jiangnan University, Wuxi, China. He is also a Postdoctoral Researcher with the Department of Electronic Engineering, Tsinghua University. His current research interest includes autonomous driving communication technology.

ZIYANG WANG (Member, IEEE) was born in Henan, China, in 1991. He received the Ph.D. degree in electromagnetic wave and microwave technology from Xidian University, Xi'an, China, in 2018. He is currently a Postdoctoral Researcher with the Department of Electronic Engineering, Tsinghua University. His research interests include 1-bit element design, phase controlled electromagnetic surface, vortex electromagnetic wave and spatial beamforming design, global optimization algorithm, 5G MIMO antenna, array antenna decoupling, and antenna broadband design.

YINGZENG YIN (Member, IEEE) received the B.S., M.S., and Ph.D. degrees in electromagnetic wave and microwave technology from Xidian University, Xi'an, China, in 1987, 1990, and 2002, respectively.

From 1990 to 1992, he was a Research Assistant and an Instructor with the Institute of Antennas and Electromagnetic Scattering, Xidian University. From 1992 to 1996, he was an Associate Professor with the Department of Electromagnetic Engineering, Xidian University. Since 2004, he has been a Professor with Xidian University. His research interests include design of microstrip antennas, artificial magnetic conductors, phased array antennas, and computer aided design for antennas.

. . .